CHARACTERIZATION OF NEUTRON IRRADIATED CANDU INCONEL X-750 SPRINGS VIA LIFT OUT THREE POINT BEND TESTS

C. HOWARD, S. PARKER, P. HOSEMANN
Department of Nuclear Engineering, University of California Berkeley
4155 Etcheverry Hall, MC 1730, Berkeley, CA 94720-1730, USA

M. GRIFFITHS, C. JUDGE, D. POFF
Canadian Nuclear Laboratories, Chalk River, Ontario, K0J 1J0, Canada

ABSTRACT

A new technique to perform in situ, miniaturized, lift-out, three point bend experiments was developed to assess the mechanical properties of Inconel X-750 material removed from the core of a CANDU reactor. Preliminary tests were performed on irradiated specimens that had spent about 14 full power service years in a CANDU reactor at two nominally different temperatures. Initial results indicate profound temperature and dose effects in matrix yield strength and ductility at room temperature.

1. Introduction

Face-centred cubic (fcc) high temperature, age-hardenable, nickel-based superalloys including Inconel X-750 provide high mechanical strength and ductility [1,2], good creep properties [3], and excellent corrosion resistance at elevated temperatures [1,2]. This combination of superior properties has made them suitable for use in nuclear reactors, specifically as fasteners (bolts) [4], centering pins, jet pump restraints, tie-rods and cladding for absorber rods in light water reactors (LWRs) as well as cable sheathing and core wires in flux detector assemblies, fuel channel garter springs, and tensioning springs in CANDU® reactors.

Due to the fact that nickel has a high cross-section for absorbing thermal neutrons and producing (n,α), (n,p) and (n,γ) reactions, irradiation in a power reactor generates a large number of displaced matrix atoms as well as H and He gas. In pressurised water reactors (PWRs) and boiling water reactors (BWRs), nickel alloy components are used in fuel assemblies that are limited to less than two years of in-core service, or they exist as peripheral components operating for the lifetime of the reactor. In CANDU reactors, nickel alloys are used as specialized components, primarily springs, both within the core and at the periphery of the core. Unlike traditional LWRs, CANDU reactors have a high thermal neutron flux in the periphery of the core region, and the nickel alloys in those positions are subject to the same degradation from thermal neutrons that exists in the core.

The long-term thermal neutron irradiation effects on high nickel containing components in both the core and periphery regions of CANDU reactors [2] is more pronounced compared to other alloys with low nickel content such as ferritic steels. Variations in temperature, neutron spectrum, and neutron flux for different components at different locations cause large variations in component performance. Although nickel alloys in PWRs and BWRs are not subjected to the same extremes of thermal neutron exposure as seen in CANDUs, operation for extended periods (life extension) means that nickel alloy performance may be impacted. Nickel alloys are

® CANDU (CANada Deuterium Uranium) is a registered trademark of Atomic Energy of Canada Limited

also used in various specialized applications involving exposure to both thermal and fast neutrons to the extent that large amounts of H and He are generated [5,6]. As a result, over the past few decades, ion irradiation studies have been performed to simulate reactor environment effects on the nickel superalloys Inconel 718 [7,8] and Inconel 600 [9]. From these studies, it is well understood that material degradation occurs via irradiation induced dislocation loops, cavities, and the dissolution of precipitates in the γ' and γ'' strengthening phases. Although the ion irradiation studies provide some support to understand the effects of neutron exposure and microstructural changes that affect component performance, they cannot adequately simulate the effects of neutron exposure because damage is induced in thin layers of material only, damage rates are higher, and transmutation effects are difficult to reproduce. At the same time the effects of neutron exposure on neutron irradiated materials cannot easily be assessed by conventional means involving mechanical testing of large standardised test specimens because of the time and effort to irradiate and then test specimens using materials test reactors. In the past 10 years, the ability to test materials that have been milled out of small or complex nuclear reactor components has provided a means of studying irradiation effects in the material that are pertinent to the reactor component and the operating conditions. In the case of nickel alloys in the CANDU reactor, irradiation temperature is a substantial factor that affects the functionality of both Inconel X-750 springs and Inconel 600 flux detectors in the CANDU reactor [10].

In this study Inconel X-750 spring material that had been operating at temperatures ~180°C and ~300°C [2] was examined. There is a large uncertainty on the operating temperature because of temperature gradients in the components [2, 10-13] so approximate mean values are used in this paper.

Post-irradiation fracture of the springs showed that failure was entirely intergranular [10, 11]. Transmission electron microscopy (TEM) investigations have confirmed the presence of helium bubbles in the matrix and aligned along grain boundaries and matrix-precipitate interfaces [10-13]. There were significant differences in the bubble microstructure between Inconel X-750 material irradiated at the two nominal temperatures, bubbles being larger and less dense at the higher temperature. The He bubble microstructure varied within a given specimen, with larger bubble sizes and higher densities on grain boundaries and matrix-precipitate interfaces, thus supporting a He-bubble mechanism for crack propagation along grain boundaries [10, 12]. Temperature affects the type, size, and distribution of dislocation loops and cavities. The low temperature specimens contain a high density of stacking fault tetrahedral and dislocation loops and a uniform density of 1-3 nm cavities, whereas 12 o'clock specimens exhibit larger dislocation loops and a more heterogeneous distribution of large cavities agglomerated along grain boundaries and phase boundaries [12, 13].

Bulk crush tests performed at Chalk River Laboratories (CRL) show that springs irradiated at the higher temperature exhibit lower strength and ductility compared to springs irradiated at the lower temperature. Irradiated specimens are initially stronger than non-irradiated specimens, but extended service results in reduced strength and ductility. The bulk crush test apparatus, crushed spring specimens, and mechanical data for springs after 14 full power years of service can be seen in Figure 2. Hardness measurements from the same specimens showed that spring material irradiated at the lower temperature are softer (340-393 VHN) compared to the hotter material irradiated at higher temperatures (400-456 VHN).

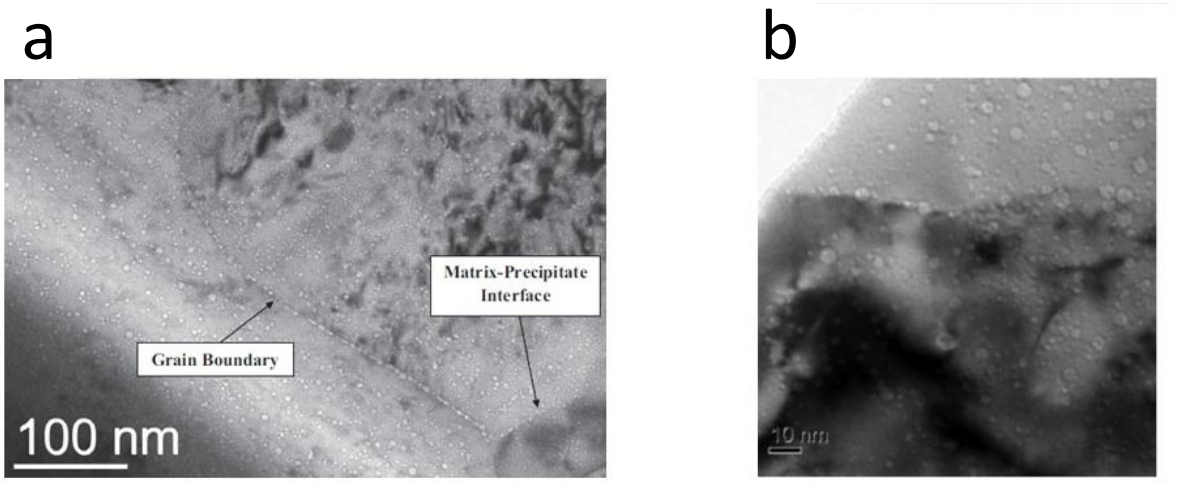

Fig 1. Inconel X-750 springs: (a) TEM micrograph depicting helium bubbles preferentially aligned along grain boundaries [12], and (b) TEM micrograph depicting cavity enrichment along a grain boundary [13].

Because the spring specimens are made with wires that are 0.7 mm thick, bulk crush testing and general conventional mechanical tests are not easily, cheaply, and safely duplicated to obtain good statistics due to the limited amount of material available. Also when sharp temperature gradients are present crush test samples may straddle a large range of operating temperatures making it difficult to assess the temperature dependence. There is also concern with both crush testing and hardness indentation testing that common metallurgical parameters that can be used to quantify the mechanical properties like ductility, yield strength, and ultimate tensile strength cannot be obtained directly.

In this study, a novel technique to perform in situ, lift-out, three point bend testing in high vacuum inside of a scanning electron microscope (SEM) on both low and high temperature specimens from an Inconel X-750 spring has been developed in order to directly link the previously observed preferential alignment of cavities and helium bubbles along grain boundaries in the TEM to quantitative changes in mechanical properties in terms of yield strength and ductility.

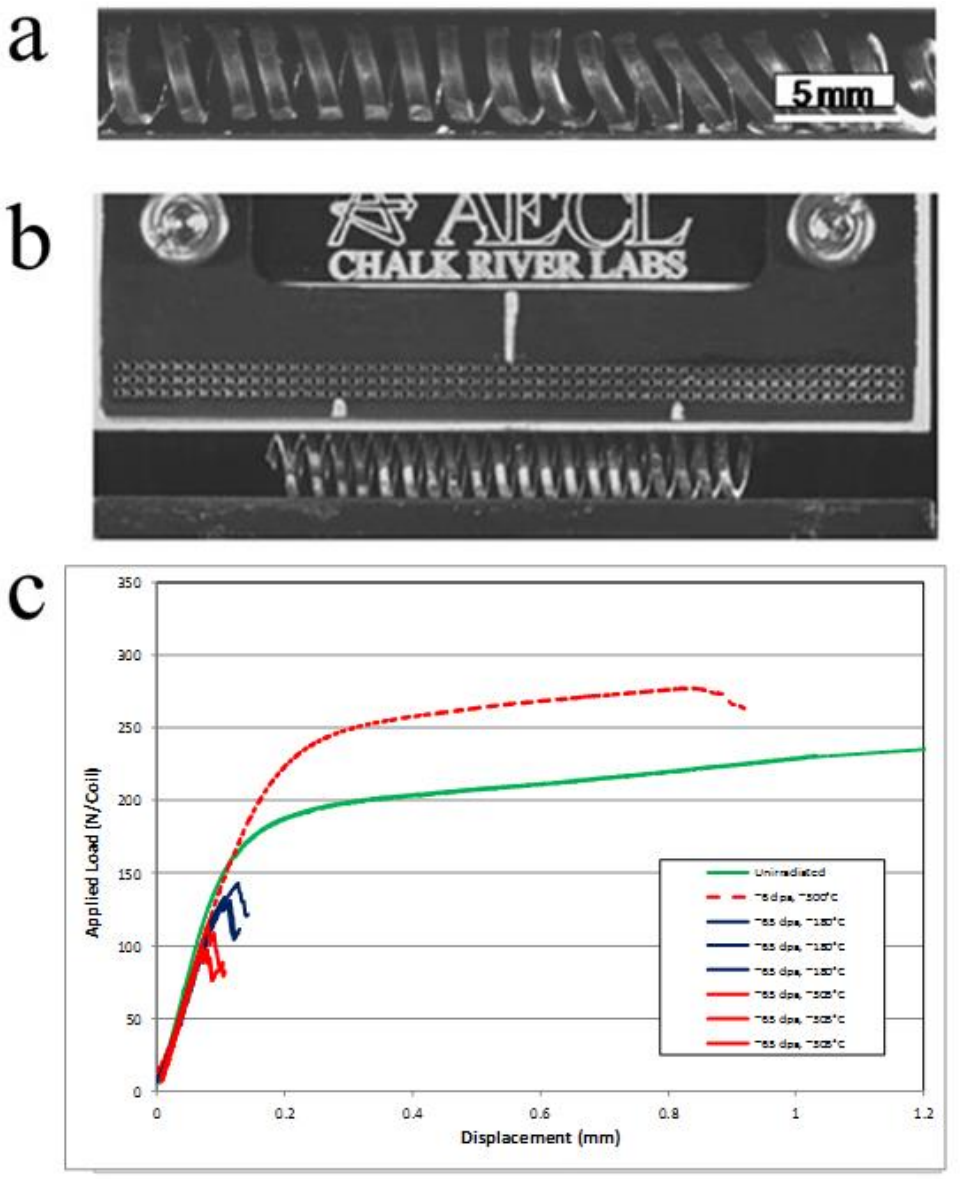

Fig 2. Bulk crush testing of Inconel X-750 garter springs: (a) post-test specimen, (b) close up view of the pre-test set up, (c) load-displacement curves of selected specimens

2. Experimental Procedures

2.1 Material

Tight-fitting CANDU springs are manufactured from Inconel X-750, a precipitation hardened variant of Alloy-600. Its chemical composition and heat treatment is shown in Table 1.

Table 1: Chemical composition in wt% and heat treatments for Inconel X-750

Element	Concentration (wt%)
Al	0.4-1
C	.08
Co	1
Cr	14-17
Cu	0.5
Fe	5-9
Mn	1
Ni	70
S	0.01
Si	0.5
Ti	2.25-2.75
Nb + Ta	0.7-1.2
Solution Treatment	1093-1204 ^{o}C
Precipitation Hardening	732 ± 14 ^{o}C for 16.5 hrs, air cool

The initial microstructure consists of 12 ± 8 µm equiaxed grains (45 µm maximum) of an fcc γ matrix with many {111} deformation twins and blocky micron-sized fcc (Ti,Nb)C inclusions that form stringers. Smaller fcc precipitates < 1 µm in size of the form $M_{23}C_6$ (90 wt% Cr) lie along grain boundaries and in grain interiors. In addition, 15 nm average sized ordered fcc γ' Ni_3Al precipitates have a different lattice parameter from the matrix by 0.5% and are non-uniformly distributed. Finally, an η-phased Ni_3Ti precipitate can be seen on grain boundaries. An EBSD scan and its corresponding Kikuchi band contrast revealing microstructure is shown in Figure 3. [14].

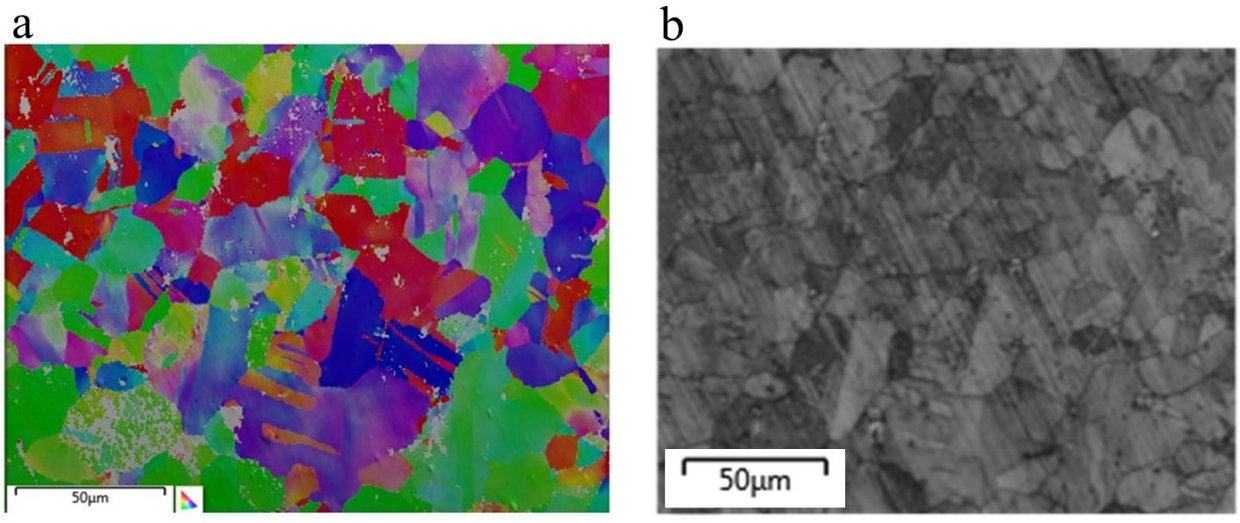

Fig 3. (a) EBSD scan and (b) Kikuchi band contrast of Inconel X-750 showing equiaxed grains with precipitates and twins.

2.2 In Service Damage and Helium & Hydrogen Production

Components in typical reactors that are in current operation are primarily damaged by direct collisions with neutrons of energies greater than 1 MeV that produce about 1 dpa for every year

of service. This equates to approximately 25 dpa by the end of a components design life. In addition to this baseline damage, nickel components encounter supplemental damage from thermal neutron absorption and subsequent transmutation reactions which more than double total damage due to additional displacement damage from ejected particles and recoils as well as large amounts of hydrogen and helium trapped in the material. Total damage is upwards of 60 dpa. Nickel in its most abundant form (68.077%) exists as ^{58}Ni and undergoes the following transmutation.

$$^{58}Ni + n \rightarrow {}^{59}Ni + \gamma \qquad (1)$$

The ^{59}Ni then emits hydrogen and helium by the following two reactions

$$^{59}Ni + n \rightarrow {}^{56}Fe + {}^{4}He \qquad (2)$$

$$^{59}Ni + n \rightarrow {}^{59}Co + {}^{1}H \qquad (3)$$

Further displacement damage also occurs by a third reaction

$$^{59}Ni + n \rightarrow {}^{60}Ni + \gamma \qquad (4)$$

The most significant contribution to total displacement damage, hydrogen, and helium production occurs via reaction (2). Over their lifetime of operation, Inconel X-750 springs in the CANDU reactor core produce >20000 appm and >5000 appm hydrogen [2].

2.3 Sample Preparation

This study focuses on Inconel X-750 spring material irradiated to approximately 55 dpa and 18000 appm helium. Materials that had been operating at temperatures ~180°C and ~300°C [2] were investigated. A FEI Quanta 3-D Focused Ion Beam (FIB) and Oxford OmniProbe at Idaho National Laboratory (INL) were used to extract one 40 µm x 20 µm x 10 µm foil of material from the bulk springs. Pre-fabricated slots were cut into copper lift-out grids using the FIB and the lifted-out foils were platinum welded in place as shown in Figure 4.

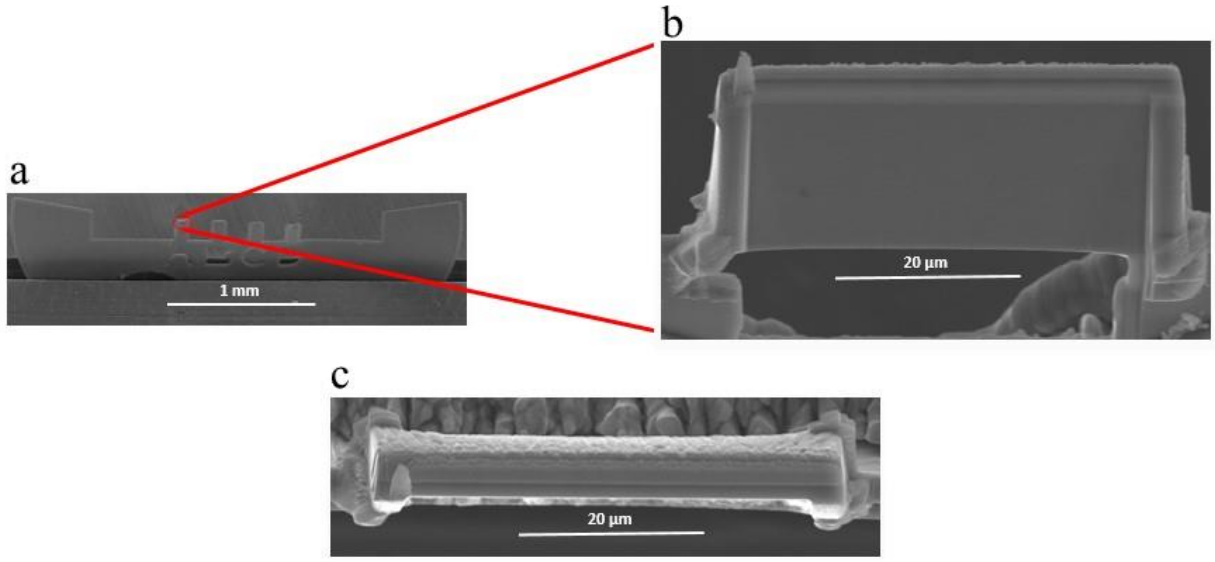

Fig. 4. Bulk extraction method of Inconel X-750 GS3 material. (a) Lift-out grid with pre-fabricated slot in position A (b) side view of large extracted foil welded into the pre-fabricated slot (c) top view of large extracted foil welded into the pre-fabricated slot

These large foils were then shipped to UC Berkeley for further preparation. Three-point bend specimens were manufactured from these large foils using an in house machined 90^{o} SEM holder inside vacuum in a FEI Quanta 3D FEG with a Ga^{69+} FIB. Initially, larger milling currents (3-7 nA) were used to cut rough bars of approximate dimensions 20 µm x 7 µm x 7 µm. This set up can be seen in Figure 5a and the resulting bar shapes cut into the large foil can be seen in Figure 5b.

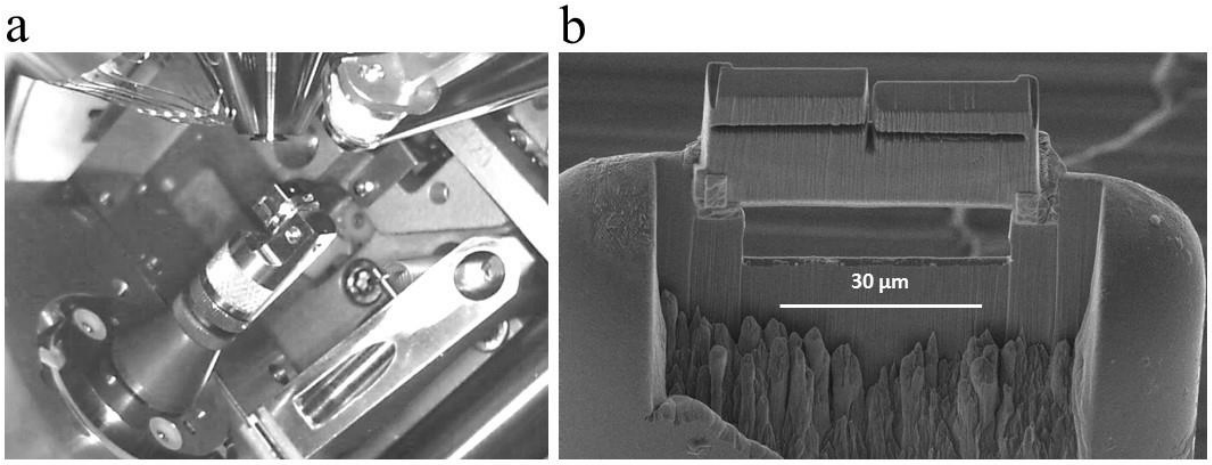

Fig. 5. (a) Manufacturing position as seen by the infrared camera showing the 90^{o} sample holder tilted 52^{o} in vacuum for milling bar structures into the large foils (b) resulting bar structures

Each bar specimen similar to the two shown in Figure 6b was subsequently lifted out using Kleindiek Nanotechnik manipulators and the FIB and platinum welded across pre-fabricated bridges. After the bars were secured across these bridges, they were FIB polished to smooth final dimensions using smaller milling currents (100 pA-1 nA). This process and an example of a finished three point bend specimen can be seen in Figure 6. Final three point bend specimens were approximately 20 µm long and 3-5 µm in width and thickness.

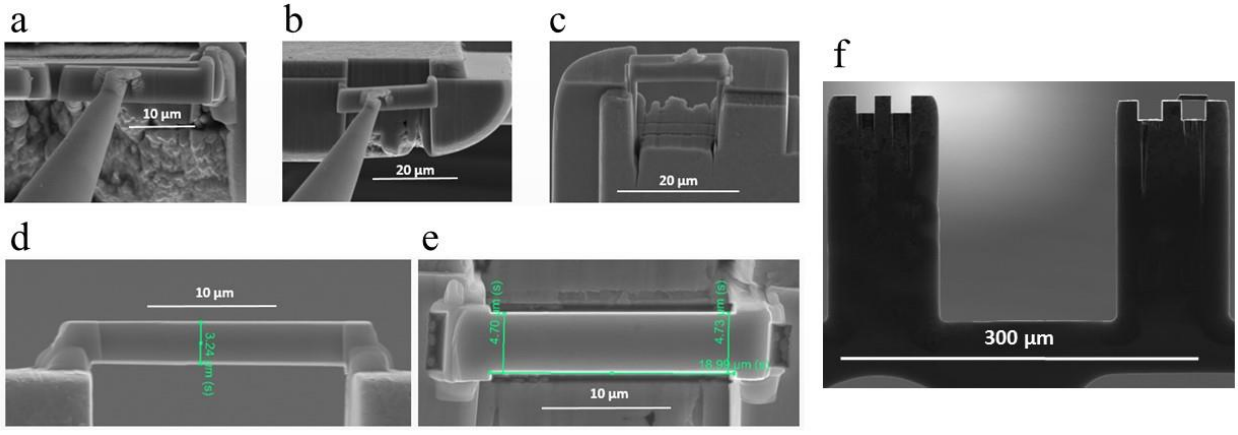

Fig. 6. (a) Three-point bend specimen lift out from extraction foil, (b) mounting across bridge testing area, (c) platinum welding to final testing position, (d) side view and (e) top view of an example final three point bend bar depicting its measured dimensions after FIB cleaning, (f) overview of pillars on lift out grid with a finished three point bend specimen mounted

All post-test specimens were subsequently thinned down to approximately 100-200 nm thickness using the FIB for high resolution imaging of the deformed material using Scanning Transmission Electron Microscopy (STEM).

2.4Electron Backscatter Diffraction (EBSD)

Electron backscatter diffraction (EBSD) was performed on both the front and top surfaces of all finished three point bend specimens using an acceleration voltage of 30 keV and electron current of 48 nA in order to map each sample's initial microstructure and identify grain boundaries. It was determined that the pinched, 6 o'clock specimens did not contain grain boundaries, but the unpinched, 12 o'clock specimens contained grain boundaries that often spanned the length and thickness of the specimen. This can be seen in Figure 7.

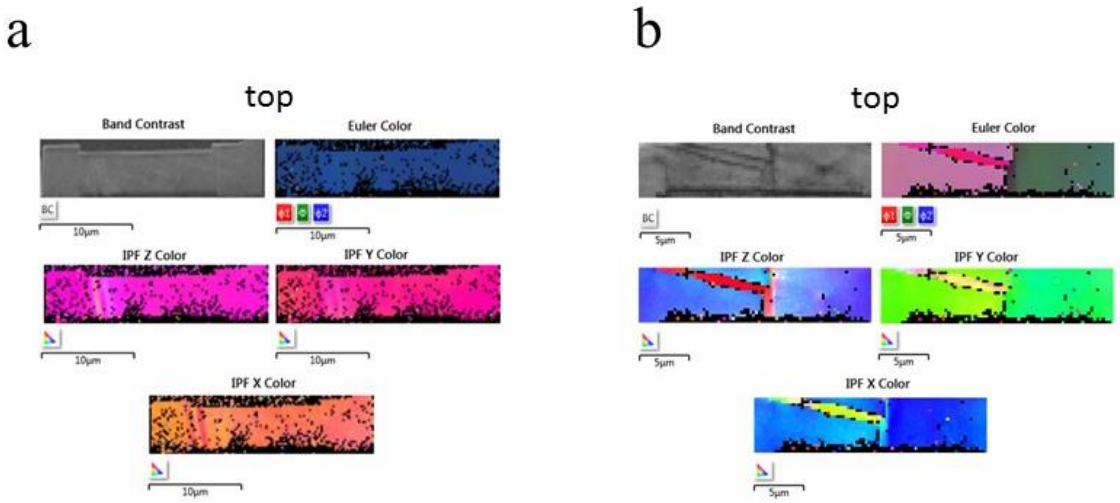

Fig. 7. Electron backscatter diffraction (EBSD) on the top surfaces of an example (a) pinched 6 o'clock specimen and (b) unpinched 12 o'clock specimen. Grain boundaries are evident in (b) but not in (a).

2.5Three Point Bend Testing

Two pinched specimens and four unpinched specimens were bent at their centre under vacuum in a Quanta 3D FEG using a Hysitron PI 85 Picoindenter with a 5 µm long diamond wedge punch. Videos were recorded for all tests for further analysis using the Scanning Electron Microscope (SEM) on the Quanta 3D FEG. All tests were performed in displacement controlled mode at loading and unloading rates of 15 nm/s to maximum strains larger than 10% or until fracture occurred. In order to ensure proper sample to tip alignment the PI 85 was tilted inside the SEM chamber to 8-15^{o} to allow simultaneous imaging of the sample and indenter with both the SEM and FIB beams. The recorded force vs. displacement curves were converted into flexural stress vs. flexural strain curves using the following equations.

$$\sigma = \frac{3\,F\,L}{2\,b\,d^2} \qquad (5)$$

$$\varepsilon = \frac{6\,D\,d}{L^2} \qquad (6)$$

F is the recorded displacement in N, L the length of the specimen in mm, b the specimen width in mm, d the specimen height in mm, D the recorded displacement at the midpoint, σ the stress at the midpoint in MPa, and ε the strain in the outer surface at the midpoint. The linear elastic loading and unloading portions of each curve were fit to linear regression lines of the form σ = Y ε + A, where σ is stress, Y is the effective pillar stiffness parameter, ε is strain, and A is an offset parameter. A 0.2% offset from this linear elastic loading regime was applied much like in ASTM tensile testing to acquire an effective specimen yield strength (σ_y). The strain on the outer fibers at this yield point was also noted as ε_y.

3. Results

The flexural stress-strain response of all six tests can be seen in Figure 8. The pinched specimens were locally strained at their midpoints to approximately double the amount of the unpinched specimens when yielding occurred, 3.4 ± 0.5 % strain versus 1.6 ± 0.3 % strain. It is also of note that the average yield stress values (0.2% offset) for the pinched specimens is 1561 ± 12 MPa, whereas the unpinched specimens yield at 1877 ± 77 MPa.

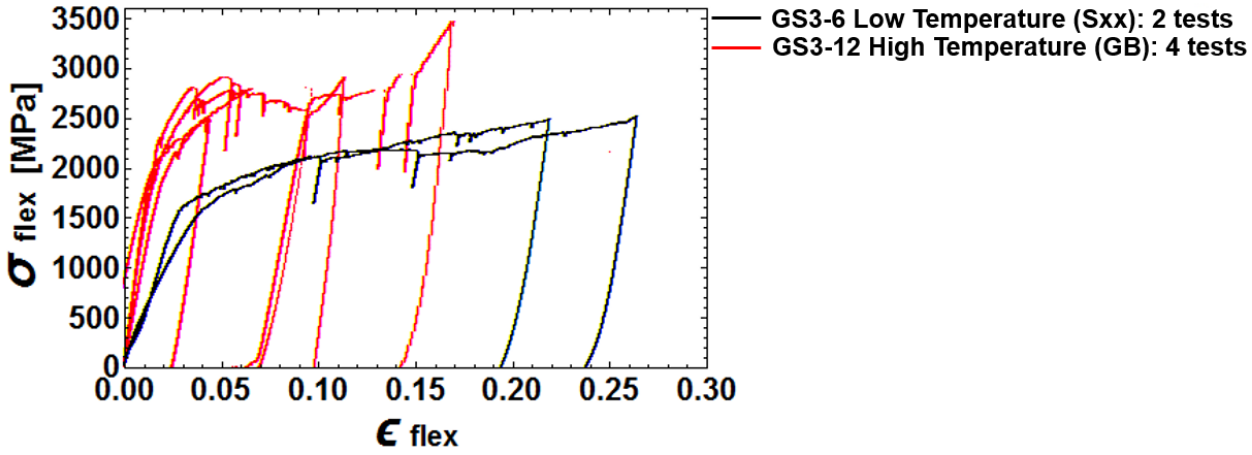

Fig. 8. Flexural stress vs. strain curves of irradiated Inconel X-750 springs.

For all tests, complete fracture of the specimens did not occur before either the platinum welds holding the bar in place broke and/or extreme bending of the specimens created contact between the side of the indenting wedge and the specimen at which point the test was stopped and unloaded. Examples of both of these can be seen in Figure 9.

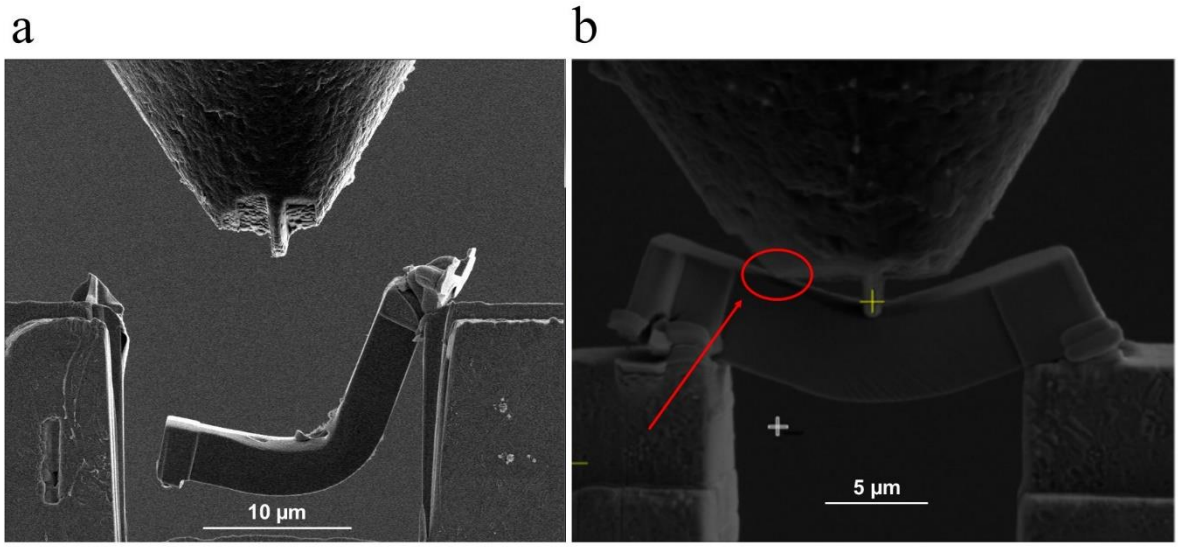

Fig. 9. SEM micrographs depicting points at which three point bend testing was stopped. (a) Platinum welds holding the sample on top of the grid have fractured causing it to fall into the empty space below. (b) After high amounts of strain, an edge of the tip above the indenting wedge has come in contact with the sample indicated in the circled region pointed to by the arrow.

The plastic deformation that takes place during the bending of all specimens is driven entirely by dislocation slip. This can be shown by the parallel slip planes seen in deformed specimens, both pinched and unpinched, as seen in real time as imaged by the SEM and in post-test STEM images shown in Figure 10.

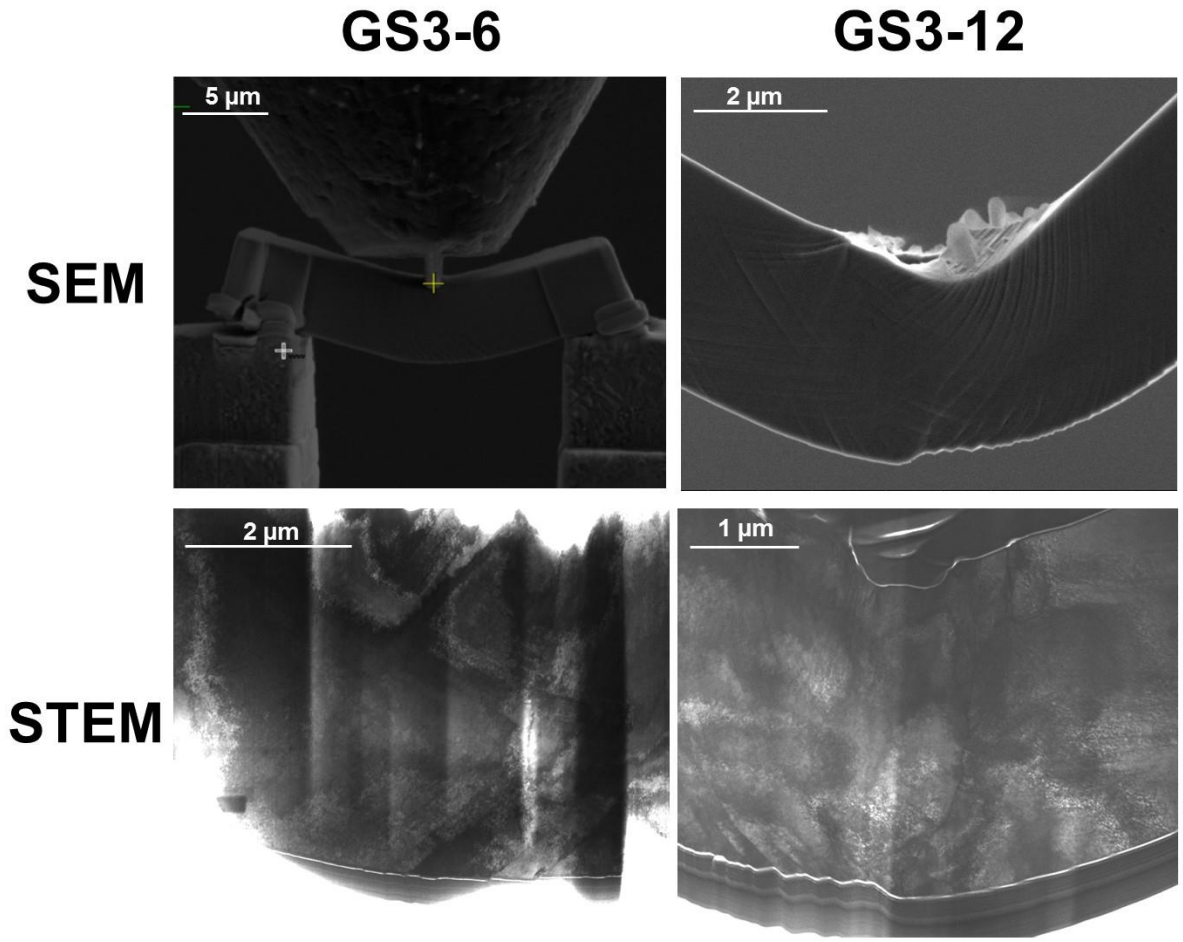

Fig. 10. SEM and STEM micrographs depicting slip planes formed during the deformation of GS3 bending specimens.

4. Discussion

The results suggest that there is an inverse relationship between temperature and yield stress. The low temperature, pinched, material yields at stress values approximately 300 MPa lower than the high temperature, unpinched material. This trend is opposite to conventional effects where radiation damage and radiation strengthening are a function of defect cluster density that decreases with higher irradiation temperature. The yield strength itself decreases with increasing test temperature except under particular conditions for some γ' containing superalloys, where the γ' precipitates with a sufficient size and density can suppress the decrease in yield strength with increasing temperature [15].

In 304 stainless steel, which has a similar vacancy migration energy to the Inconel X-750 material studied here, for irradiation doses greater than or equal to 10 dpa the steel is softer after irradiation at 200 ^{o}C compared with 300 ^{o}C. This is summarized in Figure 11 [16].

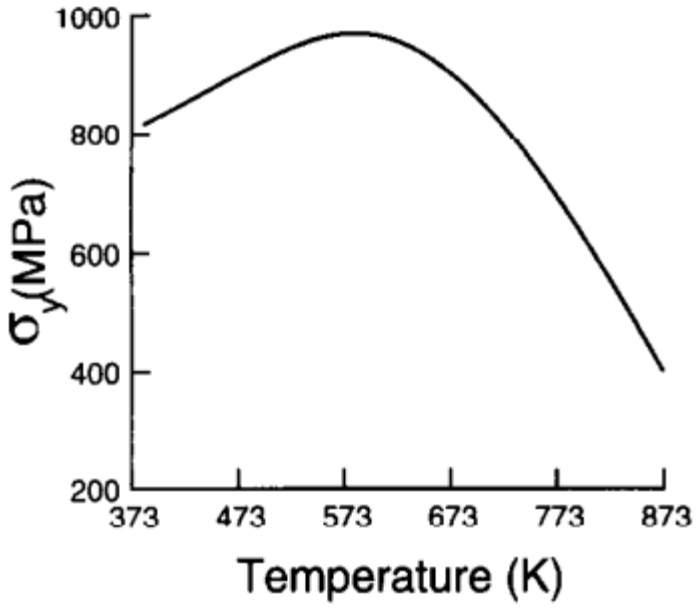

Fig. 11. The approximate variation of peak yield stress with irradiation temperature for neutron irradiated austenitic stainless steels. [16]

The yield strength for the Inconel X-750 spring material investigated here is consistent with the effects described in Figure 12. The unpinched material had an irradiation temperature of approximately 573 K, whereas the pinched material had an irradiation temperature of approximately 464 K. According to Figure 12, this difference in irradiation temperature would cause the pinched material to yield at approximately 90% of the yield of the unpinched material. Although this model has been developed for austenitic stainless steels, our Inconel X-750 pinched material yields at 83% of the unpinched material, suggesting similar effects for nickel alloys.

This inverse strength-temperature relationship is also supported by microstructural observations reported in [13]. Due to vacancy migration energies, at lower irradiation temperatures, the material is in a recombination dominated regime, whereas at higher irradiation temperatures the material is in a sink dominated regime. Thus, when interstitial clusters first form in the pinched material, they are often annihilated through recombination, whereas in the unpinched material, they survive to form dislocation loops. In addition, the lower temperature of the pinched material may allow for more disordering and dissolution of precipitate structures. Finally, cavity densities are much higher but individual cavity sizes are much smaller for the pinched material, meaning they are more evenly distributed. Overall, the matrix microstructure is much cleaner and more homogeneous in the pinched material, leaving less obstacles to be overcome during loading deformation, less necessity for dislocation climb of network dislocations, and ultimately a softer matrix material with a lower yield strength value.

The results from the in situ three point bend specimens showing a higher room temperature yield stress at higher irradiation temperatures are in agreement with room temperature hardness measurements from high fluence material that was tested by crushing (Figure 3). The failure load, (ultimate tensile strength) shows the opposite trend with temperature and this is probably because the failure load is dependent on the grain boundary strength, which is not necessarily governed by the same microstructural differences that are affecting the matrix yield strength.

Ultimately, although yielding may occur according to one temperature rule, the grain boundary failure is governed by a different rule. This ultimate failure was not observed in the three-point-bend testing because there was no suitably oriented grain boundary residing in the highest stress bearing region. This argument in favor of intergranular failure caused by helium preferentially aligning along and weakening grain boundaries is also supported by TEM investigations in [2,10-13]. The matrix strength is dominated by microstructural features other than cavities (dislocation loops and precipitates) and the radiation-induced changes in these features have a different temperature dependence [5, 6,10,12,13].

In our studies, due to a limited amount of sample volume, there is a lower probability of sampling a significant proportion of grain boundaries. Even in cases where grain boundaries were sampled in the unpinched material, they were not preferentially oriented in the center of the specimen in regions of highest stress. Thus, the reported yield strengths reflect those of the matrix properties and exclude grain boundary effects. Grain boundary effects are more easily observed in macroscopic loading numbers in bulk crush tests due to the large amount of sample volume; however yield strength values cannot be reported by this method due to imprecise measurements of sample crush areas.

A decrease in yield strength during irradiation is a phenomenon that is common to many precipitation-hardened materials. This has been linked to the effect of irradiation on dissolving and dispersing coherent matrix precipitates [5,6,10]. Although point defect clustering is likely to saturate in density at low doses [16], the precipitate dissolution occurs over much longer times and doses and the matrix microstructure may still be evolving after 50 dpa of radiation damage (the dose applicable to the specimens tested here). At the same time accumulation of He bubbles on grain boundaries also occurs over long periods of time. The dose and temperature dependence for the He bubble accumulation is established through TEM observations but is also reflected in the fracture mode that changes with dose and temperature. Although the unirradiated material fails in a completely ductile manner, fractography [17] shows that the pinched material (colder irradiation temperature) exhibits some transgranular failure at low doses (about 6-7 dpa). Higher temperature material at the same low dose and all other higher dose material tested at both temperatures fail in an intergranular fashion showing that, although yielding occurs in the matrix, the ultimate failure point is at the grain boundaries.

5. Conclusion

This study presents the development of an in situ lift out three point bending technique for quantitatively characterizing neutron irradiated CANDU-6 Inconel X-750 garter springs. Specimens have been prepared from CANDU Inconel X-750 spring material from both low temperature, pinched, and high temperature, unpinched, regions. For the high fluence samples shown in Figure 3 the matrix yield strength (hardness) was lower at the lower irradiation temperature but the failure load (indicating the grain boundary strength) was lower at the higher irradiation temperature. The three-point-bend tests conducted here are consistent with the hardness measurements. They show that the material irradiated at the lower temperature (pinched) has a yield strength 300 MPa lower than the material irradiated at the higher irradiation temperature (unpinched). This softening of the pinched material allows it to be locally strained to 3.4% before yielding occurs, whereas the unpinched micro-beams were only strained to 1.6% before yielding occurred, suggesting higher matrix ductility.

6. Acknowledgements

The authors of this manuscript would like to acknowledge Chalk River Laboratories for their donation of sample material and the Nuclear Science User Facility (NSUF) sample library at

Idaho National Lab (INL) operated through the U.S. Department of Energy (DOE) for instrument time and sample management and preparation. Grant Bickel and Don Metzger are acknowledged for useful discussion, Marc Paulseth for temperature estimates and R. Beier for hardness measurements. The authors would like to thank the CANDU Owners Group (COG) for financial support for some of this work and permission to use the data. In addition, the authors would like to thank the Biomolecular Nanotechnology Center (BNC) at the University of California, Berkeley (UCB) for the use of the FEI Quanta 3D FEG.

7. References

[1] Mills, W. J., and Bernard Mastel. "Deformation and fracture characteristics for irradiated Inconel X-750." *Nuclear technology* 73.1 (1986): 102-108.

[2] M. Griffiths. “The Effect of Irradiation on Ni-containing Components in CANDU® Reactor Cores: A Review.” *AECL Nuclear Review* Vol. 2 Num. 1 (2013).

[3] L.C. Walters and W.E. Ruther. “In-Reactor Stress Relaxation of Inconel X-750 Springs.” *J. Nucl. Mater.* 68 (1977): 324-333.

[4] Olivera, J. J., et al. *Failure of Inconel X-750 bolts of internals of the CHOOZ-A nuclear power plant*. CEA Centre d'Etudes Nucleaires de Fontenay-aux-Roses, 92 (France). Dept. d'Analyse de Surete, 1989.

[5] Sencer, Bulent H., et al. "Microstructural evolution of Alloy 718 at high helium and hydrogen generation rates during irradiation with 600–800 MeV protons." *Journal of nuclear materials* 283 (2000): 324-328.

[6] Carsughi, Flavio, et al. "Investigations on Inconel 718 irradiated with 800 MeV protons." *Journal of nuclear materials* 264.1 (1999): 78-88.

[7] Hashimoto, N., et al. "Microstructural analysis of ion-irradiation-induced hardening in inconel 718." *Journal of nuclear materials* 318 (2003): 300-306.

[8] Hunn, J. D., et al. "Ion-irradiation-induced hardening in Inconel 718." *Journal of nuclear materials* 296.1 (2001): 203-209.

[9] Kai, Ji-Jung, and R. D. Lee. "Effects of proton irradiation on the microstructural and microchemical evolution of Inconel 600 alloy." *Journal of nuclear materials* 207 (1993): 286-294.

[10] M. Griffiths, G.A. Bickel, S.A. Donohue, P. Feenstra, C.D. Judge, D. Poff, L. Walters, M.D. Wright, L.R. Greenwood and F.A. Garner, “Degradation of Ni-alloy Components in a CANDU Reactor Core”, 16th Int. Symposium on Environmental Degradation in Materials, Asheville, NC, (2013).

[11] C.D. Judge, M. Griffiths, L. Walters, M. Wright, G.A. Bickel, O.T. Woo, M. Stewart, S.R. Douglas, F. Garner, “Embrittlement of Nickel Alloys in a CANDU Reactor Environment”, in: T. Yamamoto (Ed.), Effects of Radiation on Nuclear Materials, vol. 25, ASTM International, Anaheim, CA, 2012, pp. 161–175.

[12] C.D. Judge, N. Gauquelin, L. Walters, M. Wright, J.I. Cole, J. Madden, G.A. Botton, and M. Griffiths, “Intergranular fracture in irradiated Inconel X-750 containing very high concentrations of helium and hydrogen”, Journal of Nuclear Materials 457 (2015) 165-172.

[13] H.K. Zhang, Z. Yao, G. Morin and M. Griffiths, “TEM Characterisation of In-Reactor Neutron Irradiated CANDU Spacer material Inconel X-750”, J. Nucl. Mater. 451 (2014) 88-96.

[14] O.T. Woo, et al. “The Microstructure of Unirradiated and Neutron Irradiated Inconel X750.” Microsc. Microanal. 17 (Suppl 2), 2011.

[15] R.C. Read, “The Superalloys, Fundamentals and Applications”, Cambridge University Press (2006). isbn-13 978-0-511-24546-6

[16] Lucas, G. E. "The evolution of mechanical property change in irradiated austenitic stainless steels." *Journal of Nuclear Materials,* 206-2 (1993): 287-305.

[17] C.D. Judge, C. Mayhew and M. Wright,. "Intergranular fracture in irradiated Inconel X-750 containing very high concentrations of helium and hydrogen." *Journal of Nuclear Materials,* 457 (2015): 165-172.